Boron Clusters

DOI: 10.1002/anie.200701915

Boron Cluster Cations: Transition from Planar to Cylindrical Structures**

Esther Oger, Nathan R. M. Crawford, Rebecca Kelting, Patrick Weis, Manfred M. Kappes,* and Reinhart Ahlrichs**

Experiments on mass-selected boron clusters date back more than 20 years.[1] However, only recently have experimental and theoretical methods advanced enough to allow for structural assignments over a wide range of cluster sizes. To date, most is known about boron cluster anions as a result of the pioneering work of Wang and co-workers, who used a combination of photoelectron spectroscopy and quantum chemistry to determine structures for clusters with up to 20 atoms.[2,3] Throughout this size range, B_x^- ions appear to have planar, sheet-like structures comprising webs of triangles and occasionally squares. These two-dimensional structures are often bowed and sometimes partly corrugated. This distortion is likely due to strain arising from shorter bond distances at the periphery, where atoms form stronger bonds because they have fewer bond partners. In a recent study it has been suggested that whereas the B_{20}^- ion forms the planar isomer in experiment, there is an energetically very close-lying regular-cylindrical isomer comprising two stacked ten-atom rings.[4] The recent report of the preparation and electron-microscopic characterization of 3-nm-diameter single-walled boron nanotubes[5] has led to speculations that boron clusters may assume cylindrical structures beyond a critical size. We have explored this question further by structurally probing boron cluster cations using a combination of collision cross section measurements and density functional theory (DFT) calculations.

The theoretical determination of low-energy boron cluster structures faces various problems, as is apparent from studies like those reviewed in reference [2] (e.g. B_{13}^+[6–9] and B_{20}[4,10]). Electronic structures often show multiple-reference character, which makes reliable calculations expensive or virtually impossible for systems larger than B_{20}. Even more problematic are the unusual and unexpected features of geometries, which diminish the hope of locating structures of interest by experienced guesses alone. Thus, a computational procedure is needed that is unbiased, efficient, and tolerant of multiple-reference cases. As a compromise of these requirements, we have chosen the following strategy. A first set of structures for the neutral clusters was obtained with a genetic algorithm.[11,23] This procedure required on the order of 100 generations resulting in 1000 to 2000 geometry optimizations for each B_n cluster. As this approach necessitates a low-cost procedure, we chose the DFT with the BP86 functional, which has been shown to yield reliable structure constants.[12] The relatively small def2-SVP[13] orbital and auxiliary bases were considered sufficient for this purpose.

The genetic algorithm converged rapidly for small test cases like B_6 or B_{12}, that is, 20 to 40 generations sufficed for convergence. Trial runs for larger clusters (B_{16}, B_{20}, B_{24}) failed to find some of the low-energy structures even after 80 generations. To speed up convergence, we seeded the initial population with optimized structures of double or triple ribbons, other quasi-planar (QP) structures, and cylinders (CL) with two to four rings. (The preoptimized structures were checked by a force calculation for minimum character and distorted if necessary.) This procedure provides the genetic algorithm with typical structural motifs apparent from previous work and trial calculations. As for any realistic search method, there is no guarantee that the global minimum structure has actually been found, but we have recovered all previously published structures plus additional low-energy ones.

For the final treatment, we took the entire final population of the genetic algorithm and reoptimized structures with the larger def2-TZVPP[13] orbital and auxiliary bases using the better TPSS functional[14] and the appropriate charge. All calculations were done with the TURBOMOLE package; the nonhybrid DFT calculations were carried out with the RI-DFT module.[15,24]

As a general rule, the calculations are more reliable with respect to structural parameters than energies; we have to take an uncertainty of several tenths of an electron volt into account. In order to confirm or rule out the proposed structures, we compared their collision cross sections with experimental data based on ion mobility spectrometry.[16,17] The experimental setup to determine collision cross sections has been described in detail elsewhere.[18] The cationic boron clusters are produced by laser vaporization, mass selected, injected into the drift cell filled with 7 mbar helium, and guided by an electrical field. The ions leaving the cell pass a quadrupole mass filter to remove possible fragmentation products. The drift time of the ions is monitored as a function of the ratio of the helium pressure and the drift-field strength. This time is directly connected to the collision cross section Ω_{exptl} of the ions and can typically be determined with an

[*] E. Oger, Dr. N. R. M. Crawford, R. Kelting, Dr. P. Weis, Prof. M. M. Kappes, Prof. R. Ahlrichs
Institut für Physikalische Chemie
Universität Karlsruhe
76131 Karlsruhe (Germany)
Fax: (+49) 721-608-7225
E-mail: patrick.weis@chemie.uni-karlsruhe.de
manfred.kappes@chemie.uni-karlsruhe.de
reinhart.ahlrichs@chemie.uni-karlsruhe.de
Homepage: http://www.ipc.uni-karlsruhe.de

[**] This research was supported by the Deutsche Forschungsgemeinschaft. We thank L.-S. Wang for introducing us to this issue and for helpful comments on B_x^- cluster ion sources.

Table 1: Comparison of computed energies for low-lying isomers of B_{13}^+ (Figure 1).[a]

Method	13-I	13-II	13-III	13-IV
ref. [9][b]	−322.55930		2.16	1.20
BP86	−322.26582	0.57	0.86	0.99
ZPVE[c]	0.05028	0.10	0.08	0.00
TPSS	−322.41080	0.48	0.52	0.98
TPSSh	−322.36874	0.52	0.46	1.01
B3-LYP	−322.05950	1.54	1.64	1.17
B3-LYP[d]	−322.06021	1.52	1.63	1.14
BP86	−322.59469	0.96	1.28	1.04
TPSS[e]	−322.72970	0.83	0.93	1.06
TPSSh	−322.68864	0.89	0.88	1.10
B3-LYP	−322.39078	1.94	2.08	1.21
MP2-SCS	−321.56638	0.26	1.00	1.17

[a] Energies for 13-I are in atomic units, other energies are relative to this in eV. Results are single-point energies for the BP86/def2-SVP geometry using the symmetry given in Table 2. Results in the top half of the table use the def2-SVP basis, while the bottom half uses the larger def2-TZVPP basis . [b] B3-LYP/6-311G(2d1f)//D95(d), ZPVE-corrected. [c] Zero-point vibrational energy at the BP86 level. [d] Geometry optimized with B3-LYP. [e] Further optimization of 13-I in C_{2v} with TPSS yields an energy only 300 μeV lower than the C_1-optimized structure from the genetic algorithm.

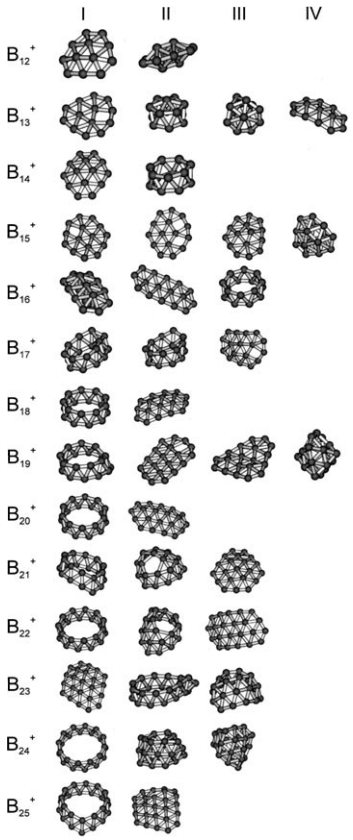

Figure 1. Relevant structures. The structures in column I correspond to the global minima; columns II–IV correspond to isomers (local minima) that are higher in energy (for relative energies, see Table 2).

Table 2: Comparison of experimental and calculated cross sections.[a]

Cluster size	Number	Symmetry/ state label	ΔE [eV]	Ω_{calcd} [Å^2]	Ω_{exptl} [Å^2]
12	I	$C_s/^2A''$	0	62.8*	63.6 ± 1.9
	II	$D_{2h}/^2A_u$	0.48	58.6	
13	I	C_{2v}	0	66.7*	66.7 ± 0.9
	II	C_{3v}	0.84	58.7	
	III	C_{3v}	0.89	59.5	
	IV	C_s	1.04	66.9	
14	I	$C_{2v}/^2A_1$	0	68.3*	69.0 ± 1.8
	II	$C_i/^2A_g$	0.08	63.7	
15	I	C_s	0	72.1*	69.4 ± 2.6
	II	C_s	0.03	72.1*	
	III	C_s	0.07	72.0*	
	IV	D_{3h}	0.12	64.3	
16	I	$C_{2v}/^2B_2$	0	68.7*	70.6 ± 0.8
	II	$C_{2h}/^2A_u$	0.07	76.6	
	III	$D_4/^2B_1$	0.09	69.6*	
17	I	C_2	0	72.2*	72.8 ± 0.6
	II	C_s	0.26	73.0*	
	III	C_1	0.36	77.5	
18	I	$C_{2h}/^2B_g$	0	75.9*	76.1 ± 0.3
	II	$C_2/^2B$	0.26	79.3	
19	I	C_s	0	79.2*	78.1 ± 1.3
	II	C_s	0.09	83.2	
	III	C_s	0.13	82.9	
	IV	C_{2v}	0.16	70.4	
20	I	$S_4/^2B$	0	82.3*	82.4 ± 1.4
	II	$C_s/^2A'$	1.09	84.8	
21	I	C_s	0	85.9	82.4 ± 1.6
	II	C_s	0.29	80.8*	
	III	C_1	0.52	86.2	
22	I	$C_{2h}/^2B_u$	0	89.1	83.2 ± 1.4
	II	$C_1/^2A$	1.08	81.7*	
	III	$C_2/^2A$	1.13	90.2	
23	I	C_{2v}	0	91.4	84.9 ± 1.8
	II	C_2	0.48	90.7	
	III	C_1	0.89	84.6*	
24	I	$C_6/^2B$	0	95.9*	94.9 ± 2.9
	II	$D_{2d}/^2A$	1.03	80.0	
	III	$C_s/^2A'$	1.31	80.7	
25	I	C_s	0	99.7*	100.6 ± 1.5
	II	C_1	0.76	97.3	

[a] For each cluster size, the global minimum structure (I) and energetically less favorable, local minimum structures (II–IV) are shown. Non-singlet-state labels are given after the point-group symmetry. ΔE is the difference in energy to the respective global minimum structure (I) calculated with TPSS/def2-TZVPP. The asterisk (*) indicates structures that are in agreement with the experimental cross section.

uncertainty of 1–2 % (see error limits in Table 2 and Figure 2). To confirm a calculated model structure, its cross section Ω_{calcd} has been calculated using the exact hard spheres scattering model[19] and compared with Ω_{exptl}. This model must be

calibrated to determine the boron collision radius, which is the only adjustable parameter. We use B_{13}^+ for calibration, since its structure is well-known,[2,6,9,20] and in our calculations it is 0.83 eV more stable than the next isomer (13-II, see Tables 1 and 2).

To give the reader an idea of methodology, and for comparison to previous work, we present in Table 1 single-point energies for the four low-lying isomers of B_{13}^+ described herein. Except as noted, the geometries were optimized with the BP86 functional and the def2-SVP basis set. Besides literature results, we provide energies for the small def2-SVP and the large def2-TZVPP basis set. The methods used DFT functionals as well as MP2-SCS, a modification of MP2 that has proven reliable even for multiple-reference cases.[21] Isomers 13-I,[6] 13-III,[7] and 13-IV[8] have been treated before; isomer 13-II appears to be new but can be formed by relaxing isomer A in reference [8] under TPSS/def2-TZVPP conditions.

The following conclusions can be drawn:

a) The present B3-LYP/def2-TZVPP relative energies agree to within 0.01 eV with a previous comparative study employing a comparable basis set,[9] and 13-I is lowest in energy for all procedures.
b) The reoptimization of structures from the BP86 geometry, as done for B3-LYP in def2-SVP, changes the relative energies of the isomers by only 0.03 eV.
c) Energies relative to isomer 13-I (ΔE) obtained with def2-SVP are obviously less reliable than those obtained with def2-TZVPP, as indicated by the larger range of ΔE values for the former.
d) The values of ΔE computed for the "planar" 13-IV differ at most by 0.17 eV among the methods tested for the larger basis.
e) B3-LYP predicts 3D structures (13-II and 13-III) to be about 1 eV higher in energy than all other methods considered, which agree to within 0.3 eV with the larger basis set (excluding MP2-SCS).
f) TPSS and its hybrid version, TPSSh, deviate by at most 0.06 eV, independent of basis set. They also agree with MP2-SCS/def2-TZVPP, with the exception of 13-II.

Since the hybrid functional TPSSh performs as well as or better than B3-LYP in standard tests,[12a] and since TPSS agrees with both TPSSh and MP2-SCS, we prefer TPSS for its much greater speed. The scatter in relative energies, even for the larger def2-TZVPP basis, is a salient reminder of the approximate nature of computational procedures applicable to systems such as B_{13}^+ and larger.

With this procedure we have proceeded to check the predicted global minimum (GM) as well as other plausible structures against experimental collision cross sections for each cluster size as follows:

B_{12}^+: The GM (12-I, Table 2, Figure 1) is a QP structure, which has been predicted by Ricca and Bauschlicher.[6] Its $\Omega_{calcd} = 62.8$ Å^2 is in agreement with the experimental value of 63.6 Å^2. The energetically second-lowest structure (12-II in Table 1 and Figure 1) is 0.48 eV higher in energy and is much more compact, with $\Omega_{calcd} = 58.6$ Å^2. This outcome is significantly below the experimental value; therefore, this structure can be ruled out.

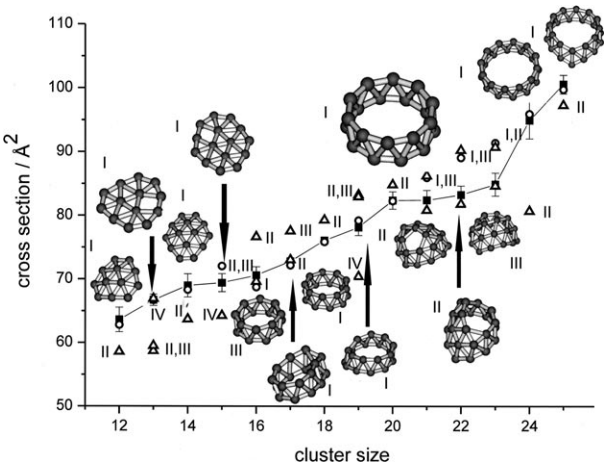

Figure 2. Comparison of calculated and experimental cross sections. ■, Error bars: Experimental values (the length of each error bar is the statistical error between the different sets of experiments). ○: Calculated global minima (also denoted I, see Figure 1 and Table 1). △: Structures that are higher in energy; the numbers II–IV refer to Figure 1 and Table 1. With the exception of B_{21}^+, B_{22}^+, and B_{23}^+, the cross sections calculated for the global minimum structures agree with the experimental values.

B_{14}^+: This GM is QP as well (14-I, $\Omega_{calcd} = 68.3$ Å^2, $\Omega_{exptl} = 69.0$ Å^2). We find in our calculations another structure (14-II) only 0.08 eV higher in energy, which consists of two stacked seven-membered rings. However, this structure can be disregarded on the basis of the collision cross section $\Omega_{calcd} = 63.7$ Å^2 (Figure 2).

B_{15}^+: We find three different QP structures within 0.07 eV (15-I, II, and III). Their Ω_{calcd} values are almost identical (72.0–72.1 Å^2) and in reasonable agreement with $\Omega_{exptl} = 69.4$ Å^2. On the basis of the cross section, we cannot distinguish among these structures, but a compact three-dimensional structure (15-IV) can be ruled out on the basis of its small $\Omega_{calcd} = 64.3$ Å^2. The lowest-energy CL structure is 0.54 eV above the GM with $\Omega_{calcd} = 66.4$ Å^2. An argument can be made, on the basis of π antiaromaticity, that the eight π electrons in planar B_{15}^+ isomers I and II should drive them to adopt a more elongated structure. The C_s structure of B_{15} in Figure 3 g,h of reference [3] would meet this condition but is 0.24 eV above the GM and leads to an unacceptably large cross section (74.3 Å^2).

B_{16}^+: For this cluster size, we again find several minima within 0.1 eV of the GM, 16-I, which has a three-dimensional, ellipsoidal structure with $\Omega_{calcd} = 68.7$ Å^2, in agreement with $\Omega_{exptl} = 70.6$ Å^2. The second-best structure (16-II) is almost planar (see Figure 1), with $\Omega_{calcd} = 76.6$ Å^2, which is clearly too large. As for B_{14}^+, we find a low-lying CL structure (16-III) only 0.09 eV above the global minimum. Its $\Omega_{calcd} = 69.6$ Å^2 agrees best with $\Omega_{exptl} = 70.6$ Å^2. We cannot distinguish between 16-I and 16-III on the basis of the collision cross section, but we can rule out the QP structure 16-II.

B_{17}^+, B_{18}^+, and B_{19}^+: In this size range we find CL structures as global minima, and their Ω_{calcd} agree with experiment. QP structures (17-III, 18-II, 19-II, 19-III) are

close in energy but can be ruled out on the basis of the cross section (see Table 2).

B_{20}^+: According to our calculations, the GM is a CL consisting of two stacked ten-membered rings (20-I). This arrangement is topologically the same structure as the GM predicted for anionic and neutral B_{20}[4,10] and deviates only slightly from idealized D_{10d} symmetry to S_4 because of Jahn–Teller distortion. In contrast to the smaller clusters, we find no other local minimum within 1 eV. Its $\Omega_{calcd} = 82.3$ Å^2 is in almost perfect agreement with $\Omega_{exptl} = 82.4$ Å^2. The next isomer (20-II) can clearly be ruled out on the basis of its cross section. There is no doubt that cationic B_{20} has a CL structure.

B_{21}^+, B_{22}^+, and B_{23}^+: For these cluster sizes, the predicted GM structures (21-I, 22-I, 23-I) are not in agreement with experiment. Instead, we assign structures (21-II, 22-II, 23-III) that are somewhat higher in energy and share the same structural motif. They can be regarded as distorted CL structures based on the B_{19}^+ CL GM structure with two, three, and four additional boron atoms forming an incomplete third ring.

B_{24}^+ and B_{25}^+: The calculation clearly favors the CL isomers (24-I, which has also been proposed by Boustani and co-workers,[22] and 25-I). These GM structures can be confirmed by their cross sections (see Table 2).

To summarize, boron cluster cations have been found to undergo a transition between quasi-planar and cylindrical molecular structures at B_{16}^+. Generally, experimentally determined collision cross sections are consistent with those calculated for GM structures as obtained from theory. For the cations B_{17}^+ and larger, cylindrical geometries dominate the low-energy structures (for neutral clusters, the transition from two-dimensional to double-ring structures occurs for B_{20}). Clusters of type B_{2n} take the form of a double ring, while B_{2n+1} merely inserts the additional boron atom into one of the rings. Jahn–Teller effects slightly distort the B_{2n} structures away from the ideal D_{nd} symmetry. Of these larger clusters, only B_{23}^+ is calculated to prefer a curved planar geometry. In this case, the experiment finds neither a planar nor the simplest double-ring-like structure. Instead, a mixed triple- and double-ring geometry appears to be favored.

Received: May 2, 2007
Revised: June 13, 2007
Published online: October 1, 2007

Keywords: boron · cluster compounds · density functional calculations · genetic algorithms · ion mobility

[1] L. Hanley, S. L. Anderson, *J. Phys. Chem.* **1987**, *91*, 5161 – 5163.
[2] A. N. Alexandrova, A. I. Boldyrev H.-J. Zhai, L.-S. Wang, *Coord. Chem. Rev.* **2006**, *250*, 2811 – 2866.
[3] H.-J. Zhai, B. Kiran, J. Li, L.-S. Wang, *Nat. Mater.* **2003**, *2*, 827 – 833.
[4] B. Kiran, S. Bulusu, H.-J. Zhai, S. Yoo, X. C. Zheng, L. S. Wang, *Proc. Natl. Acad. Sci. USA* **2005**, *102*, 961 – 964.
[5] D. Ciuparu, R. F. Klie, Y. Zhu, L. Pfefferle, *J. Phys. Chem. B* **2004**, *108*, 3967 – 3969.
[6] A. Ricca, C. W. Bauschlicher, Jr., *Chem. Phys.* **1996**, *208*, 233 – 242.
[7] I. Boustani, *Int. J. Quantum Chem.* **1994**, *52*, 1081 – 1111.
[8] R. Kawai, J. H. Weare, *Chem. Phys. Lett.* **1992**, *191*, 311 – 314.
[9] J. E. Fowler, J. M. Ugalde, *J. Phys. Chem. A* **2000**, *104*, 97 – 403.
[10] M. A. L. Marques, S. Botti, *J. Chem. Phys.* **2005**, *123*, 014310.
[11] a) D. M. Deaven, K. M. Ho, *Phys. Rev. Lett.* **1995**, *75*, 288; b) M. Sierka, J. Döbler, J. Sauer, G. Santambrogio, M. Brümmer, L. Wöste, E. Janssens, G. Meijer, K. R. Asmis, *Angew. Chem.* **2007**, *119*, 3437; *Angew. Chem. Int. Ed.* **2007**, *46*, 3372.
[12] a) V. N. Staroverov, G. E. Scuseria, J. Tao, J. P. Perdew, *J. Chem. Phys.* **2003**, *119*, 12129 – 12137; b) M. Bühl, H. Kabrede, *J. Chem. Theory Comput.* **2006**, *2*, 1282 – 1290; c) F. Furche, J. P. Perdew, *J. Chem. Phys.* **2006**, *124*, 044103.
[13] a) F. Weigend, R. Ahlrichs, *Phys. Chem. Chem. Phys.* **2005**, *7*, 3297 – 3305; b) F. Weigend, *Phys. Chem. Chem. Phys.* **2006**, *8*, 1057 – 1065.
[14] J. Tao, J. P. Perdew, V. N. Staroverov, G. E. Scuseria, *Phys. Rev. Lett.* **2003**, *91*, 146401.
[15] a) K. Eichkorn, O. Treutler, H. Öhm, M. Häser, R. Ahlrichs, *Chem. Phys. Lett.* **1995**, *240*, 283 – 290; b) M. Sierka, A. Hogekamp, R. Ahlrichs, *J. Chem. Phys.* **2003**, *118*, 9136 – 9148.
[16] G. von Helden, M.-T. Hsu, P. R. Kemper, M. T. Bowers, *J. Chem. Phys.* **1991**, *95*, 3835 – 3837.
[17] M. Jarrold, E. Bower, *J. Chem. Phys.* **1992**, *96*, 9180 – 9190.
[18] P. Weis, S. Gilb, P. Gerhardt, M. M. Kappes, *Int. J. Mass Spectrom.* **2002**, *216*, 59 – 73.
[19] A. A. Shvartsburg, M. F. Jarrold, *Chem. Phys. Lett.* **1996**, *261*, 86 – 91.
[20] F. L. Gu, X. Yang, A. C. Tang, H. J. Jiao, P. von R. Schleyer, *J. Comput. Chem.* **1998**, *19*, 203 – 214.
[21] S. Grimme, *J. Chem. Phys.* **2003**, *118*, 9095 – 9102.
[22] S. Chacko, D. G. Kanhere, I. Boustani, *Phys. Rev. B* **2003**, *68*, 035414.
[23] We employed a population size of 28–32 structures, with the number of children per generation at half the population size. The procedure was considered converged if the low-energy structures did not change for ten generations and those for higher energies for five generations.
[24] Fermi smearing (fractional orbital occupation) was used with nonsinglet initial occupation to break out of artificially imposed α–β spin symmetry and which also allows relaxation to higher spin states during the global minimum search.

